DETERMINATION OF CELESTIAL BODY PRINCIPAL AXES VIA GRAVITY FIELD ESTIMATION

Yu Takahashi* **Nicholas Bradley*** **Brian Kennedy***

The determination of physical parameters of celestial bodies provides critical navigational and scientific information. Determining the mass, rotation state, and density distribution is an important task of the navigation team on an operational mission. One representation of the internal density distribution, spherical harmonics, may be leveraged to compute the orientation of the principal axis frame of the celestial body, which in turn informs the dynamics of the body's motion. Using data from NASA's Dawn mission to the massive asteroids (1) Ceres and (4) Vesta, a method is proposed that refines the knowledge of the principal axis frame by utilizing estimated spherical harmonic coefficients. Applying an iterative rotation scheme to the solved-for body-fixed frame leads to convergence on a frame that is very close to the actual dynamical principal axis frame.

1 INTRODUCTION

Dawn is the ninth mission in NASA's competed Discovery Program, and is currently orbiting the dwarf planet Ceres. The mission goal is to better understand the formation of the early Solar System, and the asteroid belt in particular, by investigating the natural characteristics of the two largest celestial bodies in the main asteroid belt: (1) Ceres and (4) Vesta. The spacecraft carries three scientific payloads: the framing camera (FC), the visible and infrared (VIR) mapping spectrometer, and the Gamma Ray and Neutron Detector (GRaND). Gravimetry is performed by processing the radiometric tracking data received by NASA's Deep Space Network (DSN), and produces important scientific products that assist in revealing the internal structure of the body. The Dawn spacecraft visited Vesta from April 2011 to July 2012, and has been in orbit around Ceres since March 2015.

The Dawn navigation team consists of three subteams: Orbit Determination (OD), Optical Navigation (Opnav), and Maneuver Design (MD). The OD team is tasked with determining spacecraft state parameters (position and velocity), dynamic parameters (ion thruster force, solar radiation pressure, etc.), and body-specific static parameters (mass, spherical harmonic coefficients, pole direction, etc.) The available data types are radiometric (two-way Doppler and range), optical (image data processed by the Opnav team), and Delta Differential One-Way Ranging (DDOR). By filtering the available data types and iterating with the Opnav team to refine the optical data, the OD team is able to arrive at an estimate of the parameters of interest. These parameters are then delivered to the MD team, who then design the next thrust segment and the reference trajectory.

The *a priori* body frame is originally defined by the Opnav team, using image-derived estimates of the right ascension and declination of the pole vector, the prime meridian, and the rotation rate

*Outer Planet Navigation Group, Mission Design and Navigation Section, Jet Propulsion Laboratory, California Institute of Technology. 4800 Oak Grove Drive, Pasadena, California, 91109. Email: yu.takahashi@jpl.nasa.gov, nbradley@jpl.nasa.gov, brian.m.kennedy@jpl.nasa.gov

of the body. For bodies in stable rotation, such as Vesta and Ceres, the pole is coincident with the principal axis of the largest moment of inertia, and is well-defined by the body's global physical characteristics. In contrast, the prime meridian is conventionally defined with respect to a certain surface feature, such as a mountain or a crater, and has no relation to the physical characteristics or shape of the body. Because of this definition, the frame arrived at by the Opnav team is closely aligned with the principal axis in the direction of the largest moment of inertia, but is otherwise generally unrelated to the body's principal axis frame.

To obtain the orientation of the principal axis frame, we may use information gathered about the body's density distribution, represented by the spherical harmonics coefficients in any body-fixed frame. By iteratively correcting the *a priori* body-fixed frame furnished by the Opnav team, it is possible to arrive at a representation of the frame that is better aligned with the spin axis and accurately reflects the orientation of the principal axes in the body's equatorial plane. Using the principal axis frame allows for more accurate iterations with the Opnav team, and assists in mission planning by better determining the body's pole orientation. Similar work has previously been performed to estimate the rotation state of Toutatis,[1] which is in a 4:1 Earth resonant orbit. By processing the 3-1-3 Euler angles of Toutatis obtained via delay-Doppler radar images, the authors presented a direct estimate of the relative magnitudes of the moments of inertia of Toutatis to draw a conclusion about the internal density distribution of the body. Whereas the Toutatis analysis only incorporated imaging data, the purpose of the present work is to merge information obtained by radiometric data with optical measurements, providing a more accurate and robust estimate of the body's orientation.

As a final investigation, we present an assessment of the accuracy with which we need to estimate the second-degree spherical harmonic coefficients to obtain the desired accuracy in the principal axis pole and meridian location. Such analysis is useful for future planned missions to plan the orbit architecture that achieves the desired knowledge of the spherical harmonic terms.

The methods and results developed in this manuscript are applied to actual orbital data gathered by the Dawn spacecraft during both Vesta and Ceres operations, but may be applied to any celestial body for which a second degree and order gravitational field is sufficiently well-known.

2 GRAVITY FIELD DEFINITION

The gravitational potential of a body is defined via spherical harmonic expansion as follows:[2]

$$U = \frac{GM^*}{R^*} \sum_{n=0}^{\infty} \sum_{m=0}^{n} \left(\frac{R^*}{r} \right)^{n+1} P_{nm}(\sin\phi) \cdot \begin{bmatrix} \cos(m\lambda) \\ \sin(m\lambda) \end{bmatrix} \cdot \begin{bmatrix} C_{nm} \\ S_{nm} \end{bmatrix} \tag{1}$$

G is the gravitational constant, M^* and R^* are the reference mass and reference radius, P_{nm} is the associated Legendre function of degree n and order m, ϕ and λ are the latitude and longitude of the spacecraft position (r) in the body frame, and C and S are the unnormalized[†] spherical harmonic coefficients defined as

[†]Normalized spherical harmonics coefficients are more numerically stable in practical usage. Normalized coefficients may be used in the filtering process, but the mathematics behind the rotation procedure presented here assumes unnormalized coefficients. The normalized coefficients are defined as $\bar{C}_{nm} = C_{nm}/N_{nm}$, where $N_{nm} = \sqrt{\frac{(2-\delta_{0,m})(2n+1)(n-m)!}{(n+m)!}}$. The normalization for the S coefficients uses the same scaling constant N_{nm}.

$$\begin{cases} C_{nm} & = & \dfrac{(2-\delta_{0,m})}{M^*}\dfrac{(n-m)!}{(n+m)!}\displaystyle\int_M \left(\frac{r'}{R^*}\right)^n P_{nm}(\sin\phi')\cos(m\lambda')dm' \\ \\ S_{nm} & \overset{m\geq 0}{=} & \dfrac{2}{M^*}\dfrac{(n-m)!}{(n+m)!}\displaystyle\int_M \left(\frac{r'}{R^*}\right)^n P_{nm}(\sin\phi')\sin(m\lambda')dm' \end{cases} \tag{2}$$

Here, $\delta_{0,m}$ is Kronecker delta function that is zero unless m is zero, in which case it is one. The prime ($'$) denotes the quantity of the mass distribution. By direct substitution and expansion of Equation 2, the first and second-degree spherical harmonic coefficients are shown to be functions of the center-of-mass (CM) offset and the moments of inertia as:

$$\begin{cases} R^*C_{11} & = & x_{CM} \\ \\ R^*S_{11} & = & y_{CM} \\ \\ R^*C_{10} & = & z_{CM} \end{cases} \tag{3}$$

$$\begin{cases} C_{20} & = & \dfrac{1}{2M^*(R^*)^2}(I_{xx}+I_{yy}-2I_{zz}) \\ \\ C_{21} & = & -\dfrac{1}{M^*(R^*)^2}I_{xz} \\ \\ C_{22} & = & \dfrac{1}{4M^*(R^*)^2}(I_{yy}-I_{xx}) \\ \\ S_{21} & = & -\dfrac{1}{M^*(R^*)^2}I_{yz} \\ \\ S_{22} & = & -\dfrac{1}{2M^*(R^*)^2}I_{xy} \end{cases} \tag{4}$$

Accordingly, the first and second-degree gravitational potential may be individually written as

$$U_1 \quad = \quad \frac{GM^*}{r^3}\vec{r}\cdot\vec{r}_{CM} \tag{5}$$

$$U_2 \quad = \quad \frac{G}{2r^3}I_T - \frac{3G}{2r^5}\vec{r}\cdot[I]\cdot\vec{r} \tag{6}$$

I_T is the trace of the inertia tensor, and $\vec{r}_{CM}$ is the location of the center of mass with respect to the origin of the chosen frame, comprised of components x_{CM}, y_{CM}, and z_{CM}. The second

term in Equation 6 is tensorial notation and reduces to a scalar. The estimation of the non-zero first-degree gravity field is equivalent to an offset of the estimation frame from the true body center of mass. After having corrected for this offset, if non-zero off-diagonal terms are still present in the inertia tensor (i.e., non-zero C_{21}, S_{21}, and S_{22}), the OD frame and the principal axes are not aligned properly, and may be corrected by applying the procedure outlined in this manuscript. The following sections discuss the relationship between the inertia tensor and the first/second-degree spherical harmonic coefficients. The result is a scheme to rotate the body-fixed estimation frame to align with the principal axes of the body.

2.1 First-degree Harmonics and Inertia Tensor

The first-degree spherical harmonic coefficients as shown in Equation 3 represent the CM offset of the body. This offset may be corrected (i.e., nulled) simply by translating the body-fixed estimation frame center to the CM of the body. The new moments of inertia after the translation may be determined by the Parallel Axis Theorem.

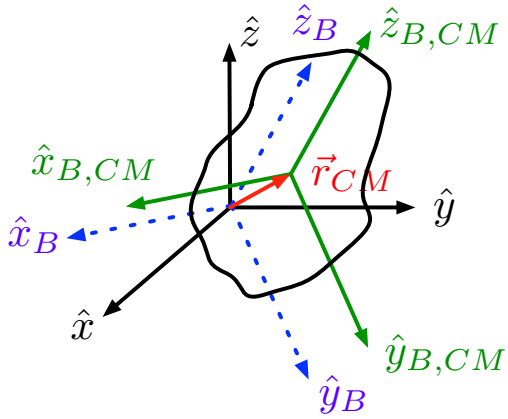

Figure 1: Estimation frame (blue) and equivalent CM-centered frame (green).

In Figure 1, the blue frame is the original coordinate frame and the green frame is the same coordinate frame centered at the CM of the body. The offset is $\vec{r}_{CM} = \left[x_{CM}, y_{CM}, z_{CM}\right]^\top$. The inertia tensor is related between frames by applying the Parallel Axis Theorem:

$$I_B = I_{B,CM} + M[\tilde{r}_{CM}][\tilde{r}_{CM}]^T \tag{7}$$

Here, M is the total mass of the body (not the reference mass) and tilde denotes the skew-symmetric matrix defined as

$$[\tilde{x}] = \begin{bmatrix} 0 & -x_3 & x_2 \\ x_3 & 0 & -x_1 \\ -x_2 & x_1 & 0 \end{bmatrix} \tag{8}$$

Thus, by direct substitution of Equation 3 into Equation 7, we arrive at the following representation of the inertia matrix in the CM-centered frame:

$$I_{B,CM} = I_B - M(R^*)^2 \begin{bmatrix} S_{11}^2 + C_{10}^2 & -C_{11}S_{11} & -C_{11}C_{10} \\ -C_{11}S_{11} & C_{11}^2 + C_{10}^2 & -S_{11}C_{10} \\ -C_{11}C_{10} & -S_{11}C_{10} & C_{11}^2 + S_{11}^2 \end{bmatrix} \quad (9)$$

It is important to note that any difference in the inertia tensors I_B and $I_{B,CM}$ is entirely due to the CM offset and not due to the misalignment between the OD frame and the principal axes, since only the first degree harmonics appear in the correction terms in Equation 9. If C_{21}, S_{21}, and S_{22} are still estimated as non-zero after this offset is applied, the body frame may be rotated into the principal axis frame by applying the coordinate transformations developed in subsequent sections. In the rest of the manuscript, we assume that the CM offset has been corrected, and the body-fixed frame has the CM as its origin.

2.2 Second-degree Harmonics and Inertia Tensor

After the CM offset is corrected, we are left with a set of spherical harmonics whose first-degree terms are zero. The rotation matrix between the principal axis frame and the estimation (OD) frame is then computed via a rotation that utilizes the non-zero second-degree harmonics. If we knew the values of the inertia tensor (or the ratios of the moments of inertia to some constant), the rotation matrix that maps from the OD frame to the principal axis frame would be easy to find. However, the inertia tensor for a principal axis rotator is unobservable,[1] and we may only estimate the five second-degree harmonic coefficients. The rotation matrix is defined by the eigenvectors of the inertia tensor that is comprised of six independent elements; since we may only directly estimate five second-degree spherical harmonic coefficients, we are left with an underdetermined system. This problem did not occur when we corrected for the center-of-mass offset because we may estimate three first-degree harmonic coefficients to solve for three coordinates of the center of mass, which is a one-to-one parameter mapping.

In order to circumvent this apparent problem of an underdetermined system, we first denote the inertia tensor in the OD frame as follows:

$$I = A + \frac{I_T}{3} 1_{[3\times3]} \quad (10)$$

The 3x3 identity matrix is denoted $1_{[3\times3]}$, and the matrix A consists of six independent components as follows:

$$A = \begin{bmatrix} K_1 & I_{xy} & I_{xz} \\ I_{xy} & K_2 & I_{yz} \\ I_{xz} & I_{yz} & K_3 \end{bmatrix} \quad (11)$$

We note that the diagonalization of I is equivalent to the diagonalization of A, since the second term in Equation 10 already diagonalized. That is, if we define Q as the rotation matrix that diagonalizes I, where $QQ^\top = 1_{[3\times3]}$, the resulting diagonal matrix I_D is obtained as follows:

$$I_D = QIQ^\top = Q(A + \frac{I_T}{3} 1_{[3\times3]})Q^\top = QAQ^\top + \frac{I_T}{3} 1_{[3\times3]} \quad (12)$$

The diagonal components K_i are computed as:

$$K_1 = I_{xx} - \frac{I_T}{3} = \frac{(I_{xx} - I_{yy}) + (I_{xx} - I_{zz})}{3} = \frac{(C_{20} - 6C_{22})}{3} M^*(R^*)^2 \quad (13)$$

$$K_2 = I_{yy} - \frac{I_T}{3} = \frac{(I_{yy} - I_{xx}) + (I_{yy} - I_{zz})}{3} = \frac{(C_{20} + 6C_{22})}{3} M^*(R^*)^2 \quad (14)$$

$$K_3 = I_{zz} - \frac{I_T}{3} = \frac{(I_{zz} - I_{xx}) + (I_{zz} - I_{yy})}{3} = \frac{-2C_{20}}{3} M^*(R^*)^2 \quad (15)$$

Thus, the matrix A may be expressed in terms of the second-degree spherical harmonics as

$$A = \begin{bmatrix} \frac{(C_{20} - 6C_{22})}{3} & -2S_{22} & -C_{21} \\ -2S_{22} & \frac{(C_{20} + 6C_{22})}{3} & -S_{21} \\ -C_{21} & -S_{21} & \frac{-2C_{20}}{3} \end{bmatrix} M^*(R^*)^2 \quad (16)$$

A right-handed rotation matrix Q composed of the eigenvectors of A will yield the correct rotation from the OD frame (in which the harmonics are estimated) to the principal axis frame (in which the inertia tensor is diagonalized). This formulation eliminates the need to determine the full inertia tensor, and all further analysis may be conducted by estimating the five second-degree spherical harmonic coefficients.

The multiplication by $M^*(R^*)^2$ in Equation 16 only changes the scaling of the eigenvalues and does not affect the eigenvectors. In the procedures and results presented here, we operate on an A matrix without the trailing scalar multiplier.

3 FRAME DEFINITIONS

A coordinate frame of a celestial body in stable rotation is defined by the right ascension (RA, or α), declination (Dec, or δ), prime meridian at a particular epoch (W_0), and the rotation rate (ω). The RA and Dec define the orientation of the pole in the inertial frame and the prime meridian defines the orientation of the body xy-axes. The prime meridian angle at any given time t is defined as:

$$W(t) = W_0 + \omega(t - t_0) \quad (17)$$

We refer to W as the prime meridian angle, and W_0 as the prime meridian at epoch t_0. Thus, the prime meridian angle W is tied to a particular epoch and the rotation rate ω.

With these angular definitions, we may now define three different operational frames: The Opnav frame (which is solved for by the Opnav team), the OD frame (which is solved for by the OD team using Opnav and other data types), and the principal axis frame. Each of these frames may be related to the inertial EME2000 reference frame through various rotation matrices. Figure 2 depicts how the four frames are related to each other. The following subsections develop the rotation matrices used to switch between coordinate frames.

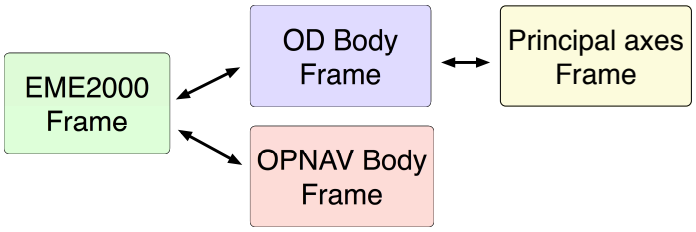

Figure 2: Coordinate frame relationships.

3.1 Inertial (EME2000) to the OD Body Frame

First, we describe the rotation between the inertial frame (EME2000, or *I* frame) and the OD frame (*p* frame). The OD frame is solved for in the filtering process using radiometric and Opnav data, and in general has non-zero C_{21}, S_{21}, and S_{22} values. Figure 3 depicts the rotation between the *I* and *p* frames, where the *I* frame axes are denoted by XYZ and the *p* frame axes are denoted by xyz.

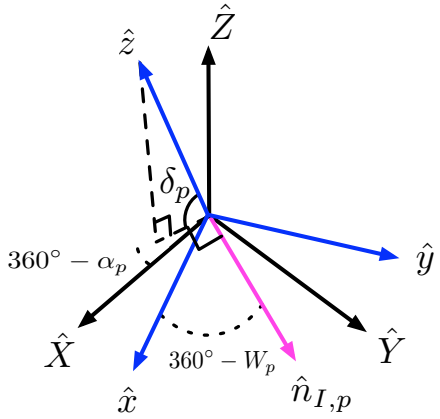

Figure 3: Inertial EME2000 (XYZ) and OD Body Frame (xyz).

The $\hat{z}$ axis is defined by the filter's estimate of α_p and δ_p in the EME2000 frame. This pole vector may be expressed in either coordinate frame, where a preceding superscript indicates the frame in which the vector is being expressed:

$$ {}^{p}\hat{z} = \begin{bmatrix} 0 \\ 0 \\ 1 \end{bmatrix} \tag{18} $$

$$ {}^{I}\hat{z} = \begin{bmatrix} \cos\delta_p \cos\alpha_p \\ \cos\delta_p \sin\alpha_p \\ \sin\delta_p \end{bmatrix} \tag{19} $$

Now, let the the node vector $\hat{n}$, which is common to both the xy- and XY-planes, be defined as:

$$ {}^{I}\hat{n}_{I,p} = \frac{{}^{I}\hat{Z} \times {}^{I}\hat{z}}{\left| {}^{I}\hat{Z} \times {}^{I}\hat{z} \right|} \tag{20} $$

Since $\hat{n}_{I,p}$ is orthogonal to both $\hat{Z}$ and $\hat{z}$, it defines the crossing of EME2000 XY-plane and the OD frame's xy-plane, and its right ascension is $\alpha_p + 90^\circ$. W_p is the meridian angle between ${}^{I}\hat{n}_{I,p}$ and $\hat{x}$, measured counterclockwise positive about $\hat{z}$. The full rotation from EME2000 to the OD frame is performed through a 3-1-3 Euler angle rotation sequence. The first rotation is positive rotation about the third axis by $\alpha_p + 90^\circ$ (aligns the first axis with the node), the second rotation is a positive rotation about the first axis by $90^\circ - \delta_p$ (aligns the third axis with the pole vector). The third rotation is positive rotation about the third axis by meridian W_p (aligns the node vector with the $\hat{x}$ vector). The full rotation from the EME2000 (*I*) to the OD frame (*p*) is given by:

$$ R_{I \to p} = R_3(W_p) R_1(90^\circ - \delta_p) R_3(\alpha_p + 90^\circ) \tag{21} $$

where $R_1(\theta)$ and $R_3(\theta)$ are defined as

$$ R_1(\theta) = \begin{bmatrix} 1 & 0 & 0 \\ 0 & \cos\theta & \sin\theta \\ 0 & -\sin\theta & \cos\theta \end{bmatrix} \tag{22} $$

$$ R_3(\theta) = \begin{bmatrix} \cos\theta & \sin\theta & 0 \\ -\sin\theta & \cos\theta & 0 \\ 0 & 0 & 1 \end{bmatrix} \tag{23} $$

3.2 Inertial (EME2000) Frame to Opnav (B) Frame

The rotation from the inertial EME2000 frame to Opnav frame (*B* frame, with basis axes denoted by abc) is necessary to relate the Opnav (*B*) frame to the OD (*p*) frame. The rotation, depicted in Figure 4, is identical to the $R_{I \to p}$ rotation, but uses the Opnav-derived values for right ascension (α_B), declination (δ_B), and meridian at epoch (W_B).

$$ R_{I \to B} = R_3(W_B) R_1(90^\circ - \delta_B) R_3(\alpha_B + 90^\circ) \tag{24} $$

3.3 OD Frame to Principal Axes Frame

The rotation from the OD frame to the principal axis frame ($x'y'z'$, or the p' frame) is depicted in Figure 5 and makes use of the derivation discussed in Section 2.2. To obtain the correct rotation matrix, the eigenvalues and eigenvectors of the A matrix from Equation 16 are needed. The correct rotation matrix involves three steps:

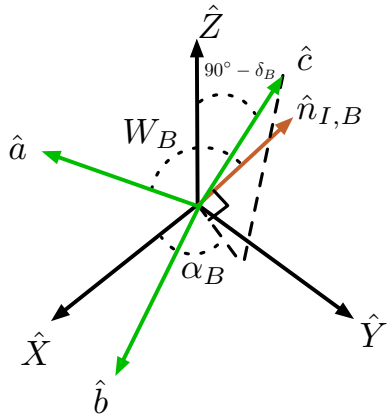

Figure 4: Inertial EME2000 (XYZ) and Opnav Frame (abc).

1. First, we reorganize the eigenvalues in ascending order of magnitude and rearrange the eigenvectors column-wise in this order. Re-ordering the eigenvectors ensures that the resulting inertia tensor is rearranged so that diagonal terms are in increasing size. This orientation is the natural rotation mode for a body in principal axis rotation.

2. Next, we assume that the estimation of the pole in the OD frame is close to the actual pole vector of the body, since observations even with Earth-based assets can determine the pole orientation of a relatively large body to within several degrees. Therefore, it is appropriate to ensure that the third component of the z-eigenvector is close to unity. If it is close to negative unity, we change the sign of the entire vector.

3. Finally, we check if the eigenvectors represent a right-handed rotation (i.e, $\vec{u}_1 \times \vec{u}_2 = \vec{u}_3$). If not, change the sign of either the x-eigenvector or y-eigenvector. Doing so will ensure that the resulting frame is either an $x - y - z$ system or $(-x) - (-y) - z$ system. These systems both represent valid principal axis frames, with their meridians shifted by $180°$ from each other. Either frame is aligned properly with the body's principal axes.

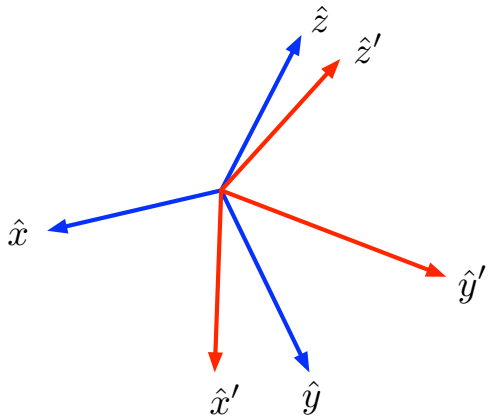

Figure 5: OD Body Frame (xyz) and Principal Axis Frame ($x'y'z'$).

The corresponding rotation from p frame to p' frame and the diagonalized inertia tensor I_D are given by:

$$R_{p\to p'} = \begin{bmatrix}\hat{u}_1 & \hat{u}_2 & \hat{u}_3\end{bmatrix}^T \tag{25}$$

$$I_D = \begin{bmatrix} I_{D,1} & 0 & 0 \\ 0 & I_{D,2} & 0 \\ 0 & 0 & I_{D,3} \end{bmatrix} \tag{26}$$

In the above, $\hat{u}_{1,2,3}$ are the eigenvectors along the x, y, and z-axes corresponding to the moments of inertia $I_{D,1}$, $I_{D,2}$, and $I_{D,3}$ where $I_{D,1} \leq I_{D,2} < I_{D,3}$. The actual values of the moments of inertia are unobservable, and are not important for the determination of the principal axis frame.

For all rotations derived thus far, the opposite rotation may be performed simply by transposing the rotation matrix (e.g., $R_{p'\to p} \equiv R_{p\to p'}^{\top}$).

3.4 Pole and Meridian Representation for the Principal Axes Frame

In the final analysis, we desire to compare the pole and meridian values solved by performing this principal axis rotation scheme to the values determined by the OD and Opnav teams. To do so, we need a rotation matrix to represent the principal axis frame (p') in the inertial EME2000 frame (I). The conversion requires the inertial representation of the principal axis pole vector ${}^I\hat{z}'$ and node vector ${}^I\hat{n}_{I,p'}$:

$${}^I\hat{z}' = R_{p\to I} R_{p'\to p} \begin{bmatrix} 0 \\ 0 \\ 1 \end{bmatrix} \tag{27}$$

$${}^I\hat{n}_{I,p'} = \frac{{}^I\hat{Z} \times {}^I\hat{z}'}{\left| {}^I\hat{Z} \times {}^I\hat{z}' \right|} \tag{28}$$

The components of the pole vector ${}^I\hat{z}'$ may be used to determine the right ascension and declination of the pole of the principal axis frame:

$$\alpha_{p'} = \tan^{-1}\left(\frac{{}^I\hat{z}'_2}{{}^I\hat{z}'_1}\right) \tag{29}$$

$$\delta_{p'} = \sin^{-1}\left({}^I\hat{z}'_3\right) \tag{30}$$

The meridian may be found by determining the node and computing the angle between it and the x-axis of the principal axis frame, which is computed as:

$$ {}^{I}\hat{x}' = R_{p\to I} R_{p'\to p} \begin{bmatrix} 1 \\ 0 \\ 0 \end{bmatrix} \tag{31} $$

With the x-axis of the principal axis frame represented in the inertial frame, the meridian is computed as:

$$ W_{p'} = \cos^{-1}\left({}^{I}\hat{x}' \cdot \hat{n}_{I,p'}\right) \tag{32} $$

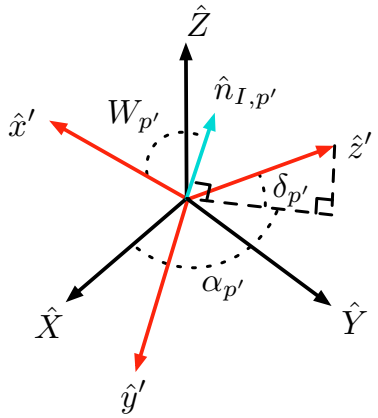

Figure 6: Inertial Frame (XYZ) and the Principal Axis Frame ($x'y'z'$).

4 ROTATION INTO THE PRINCIPAL AXIS FRAME

Once the principal axis frame orientation is determined by applying the appropriate rotations, the inputs used to generate the rotations must be themselves rotated into the new frame. The subsequent observations, expressed in the new body-fixed frame, may be re-filtered in an iterative fashion to arrive at a converged representation of the principal axis frame. Landmarks, which are control points utilized by the Opnav team, must be expressed in the new frame. Additionally, the spherical harmonics themselves must be rotated into the new frame.

4.1 Landmarks in the Principal Axis Frame

The Opnav and OD processes make extensive use of "landmarks" in filtering and estimation of state and body parameters. Landmarks are not correlated to prominent features on the surface, but are representative of locations mapped in a systematic fashion around the surface of the target body. Landmarks are an important component in determining range to the target body, which strongly influences estimates of state and gravitational parameters.

When the principal axes are found through the rotation procedures described previously, the landmarks that were previously described in the Opnav (B) frame must be rotated into the new principal axis (p') frame. Landmark rotation is accomplished by applying three successive rotations as follows, where ${}^{B}\vec{r}$ represents the landmark location in the original Opnav frame.

$$ {}^{p'}\vec{r} \;=\; R_{p\to p'} R_{I\to p} R_{B\to I}\, {}^{B}\vec{r} \tag{33} $$

Since the Opnav team generates the landmarks using their own frame and the new principal axis frame is not tied directly to the Opnav frame, we include the landmark positions as estimated parameters in the filter for each iteration. For successive iterations of the principal axis rotation algorithm, the rotated landmarks must be used as new *a priori* landmark locations. In the filter setup, the *a priori* landmark location covariance values are scaled from the Opnav estimate of the landmark uncertainty. We globally scale all the Opnav-delivered 1-sigma uncertainty values by a sufficiently large scale factor. Doing so preserves the relative positional constraints of the surface topology, but gives the filter sufficient flexibility so that the estimation process is not negatively influenced by potentially over-confident formal 1-sigma values. A typical scale factor will allow for several kilometers of uncertainty in the landmark location at a 1-sigma level for a Vesta- or Ceres-sized target body. Due to expensive filtering requirement of the landmark estimation (each landmark estimated adds three new position parameters to the estimation state vector), the total number of the landmarks is limited to a few hundred geographically representative points (< 500).

4.2 Spherical Harmonics in the Principal Axis Frame

The spherical harmonics defined in Equation 2 are body-frame specific. Therefore, along with the landmark coordinates, the estimated spherical harmonics need to be rotated into the principal axis frame to be used as *a priori* nominal values for the next iteration.

4.2.1 z-axis Rotation of Spherical Harmonics

Performing a full rotation of spherical harmonics is difficult when the direction of the pole vector changes between frames. The difficulty is due to the latitude of the differential mass component changing in Equation 2. It is not straightforward to compute $P_{nm}[\sin(\phi + \Delta\phi)]$ from the existing values of $P_{nm}(\sin\phi)$. In contrast, a rotation around a fixed z-axis is quite simple. If only a z-axis rotation is desired, we may apply a simplified rotation to the *a priori* estimate of the spherical harmonics, rotating by an angle equal to the change in meridian ($\Delta W = W_{p'} - W_p$). Since body-fixed longitude λ does not appear in the Legendre polynomial P in Equation 2, only the cosine and sine term coefficients need to be altered.

The x and y axes of the principal axis frame are rotated from the original OD frame values by:

$$ \begin{bmatrix} x' \\ y' \end{bmatrix} \;=\; \begin{bmatrix} \cos\Delta W & \sin\Delta W \\ -\sin\Delta W & \cos\Delta W \end{bmatrix} \begin{bmatrix} x \\ y \end{bmatrix} \tag{34} $$

Unless the translation of the coordinate center is involved (and we have assumed that it is not), the radial distance r is the same in both frames, and the differential mass is unchanged. Noting that $r'\cos\phi' = r\cos\phi$, we substitute and obtain:

$$ \begin{bmatrix} \cos\lambda' \\ \sin\lambda' \end{bmatrix} \;=\; \begin{bmatrix} \cos\Delta W & \sin\Delta W \\ -\sin\Delta W & \cos\Delta W \end{bmatrix} \begin{bmatrix} \cos\lambda \\ \sin\lambda \end{bmatrix} \tag{35} $$

Equation 35 states that when the meridian changes by a positive rotation of ΔW, it is equivalent to the mass distribution shifting by $-\Delta W$ in the original coordinate frame. Thus, $\lambda' = \lambda - \Delta W$, and the cosine and sine terms directly alter the C and S coefficients of the spherical harmonic expansion in Equation 2. Therefore, the spherical harmonics in the principal axis frame (C'_{nm}, S'_{nm}) are expressed as

$$\begin{bmatrix} C'_{nm} \\ S'_{nm} \end{bmatrix} = \begin{bmatrix} \cos(m\Delta W) & \sin(m\Delta W) \\ -\sin(m\Delta W) & \cos(m\Delta W) \end{bmatrix} \begin{bmatrix} C_{nm} \\ S_{nm} \end{bmatrix} \tag{36}$$

4.2.2 Full Rotation of Spherical Harmonics

When the full rotation of the spherical harmonics is desired, we find an unlikely parallel in the animation and computer graphics research community, where spherical harmonics are used to model animated lighting sources. Extensive research has been conducted to determine the mathematical representation of rotating lighting sources modeled as spherical harmonic expansions.

To the authors' knowledge, Wigner[3] was the first to formulate the idea of coordinate transformation of spherical harmonics. Since the radial distance is not affected by the coordinate transformation, the rotation of the spherical harmonic function $Y_{nm} = P_{nm}(\sin\phi) \begin{bmatrix} \cos(m\lambda) \\ \sin(m\lambda) \end{bmatrix} \equiv P_{nm} e^{im\lambda}$ (where i is the imaginary number) is all that is required (see Equation 2). Because the spherical harmonics functions are mutually orthogonal, the spherical harmonics in the new frame become a linear combination of the original spherical harmonics of the same degree. Equation 37 illustrates this linear combination.

$$\begin{bmatrix} C'_{nm} \\ S'_{nm} \end{bmatrix} = \sum_{l=0}^{n} \begin{bmatrix} \zeta^c_{nl} \\ \zeta^s_{nl} \end{bmatrix} C_{nl} + \sum_{l=1}^{n} \begin{bmatrix} \eta^c_{nl} \\ \eta^s_{nl} \end{bmatrix} S_{nl} \tag{37}$$

In the above relationship, l is a dummy variable for the order m. The coefficients ζ_{nl} and η_{nl}, with the superscript denoting which of the C and S harmonic coefficients they correspond to, are computed by a combination of z-y-z rotation (not the z-x-z rotation commonly used in the astrodynamics community). As stated earlier, the z-axis rotation is quite simple. The y-axis rotation can be computed by a direct method,[3–5] recursive formulation[5–8] or by decomposing the y-axis rotation into successive rotations of x and z-axis rotations.[9] All of these methods are esoteric and laborious to work with. Fortunately, there exists a public tool for this purpose that alleviates the labor. SHTOOLS[10] integrates with Fortran 95 or Python and can perform the coordinate rotation of the spherical harmonic coefficients seamlessly for the normalized coefficients (the same normalization introduced in the footnote in Section 2). The subsequent analysis uses the SHTOOLS exclusively, but unpublished results confirm that the simple rotation by change in meridian (Section 4.2.1) yields similar results when the assumed *a priori* pole is very close to the principal axis pole.

5 PROCEDURE

With the mathematical background in place, we present a procedure in Algorithm 1 for obtaining an improved estimate of the principal axis frame of a celestial body given an *a priori* frame and sufficiently well-estimated second-degree gravitational harmonic terms.

Algorithm 1 Iterative procedure for determining the principal axis frame of a celestial body

1: Given *a priori* estimates of the parameters of the system, converge a normal OD solution using Opnav-provided landmarks and/or radiometric tracking data
2: **while** Change in RA, Dec, and meridian is above a desired threshhold **do**
3: Form the A matrix from the unnormalized estimated spherical harmonics (Equation 16) (See footnote in Section 2)
4: Find $R_{p\to I}$ (Equation 21)
5: Find $R_{B\to I}$ (Equation 24)
6: Find the Eigenvalues and Eigenvectors of A, and use them to generate $R_{p\to p'}$ (Equation 25)
7: Solve for the updated RA ($\alpha_{p'}$) and Dec ($\delta_{p'}$) (Equations 29 and 30)
8: Solve for the updated meridian ($W_{p'}$) (Equation 32)
9: Rotate the landmarks into the new frame (Section 4.1)
10: Rotate the solved-for harmonics into the new frame (Section 4.2)
11: Run the filter with the new *a priori* inputs just computed, and compare the result (α_p, δ_p, W_p) with the new frame ($\alpha_{p'}$, $\delta_{p'}$, $W_{p'}$)
12: **if** Tolerance is not met **then**
13: Continue iteration, using the new frame, rotated landmarks, and rotated harmonics as *a priori* values
14: **else**
15: Exit iteration

Note that although the A matrix is constructed using unnormalized coefficients, the normalized coefficients can be estimated in the filter as long as they are converted appropriately for the rotation analysis.

In addition to monitoring convergence based on the relative change in RA, Dec, and meridian between iterations, one may also monitor the change in the second-degree spherical harmonics. As the solved-for frame converges on the principal axis frame, the inertia tensor will become diagonalized, and the off-diagonal components of the A matrix in Equation 16 will vanish. When convergence is achieved, $C_{21} = S_{21} = S_{22} = 0$ will be satisfied to within some tolerance. In the following results, the convergence tolerance was chosen to be 0.01° for RA, Dec, and meridian.

6 RESULTS

6.1 Vesta Results

The Dawn spacecraft orbited Vesta from April 2011 to July 2012 in six different stages. In order, Dawn proceeded through the approach phase, rotational characterizations, Survey orbit, High Altitude Mapping Orbit (HAMO), Low Altitude Mapping Orbit (LAMO), and the second High Altitude Mapping Orbit (HAMO2).[11–14] The highest resolution gravity data was available from the lowest orbit, which was LAMO. The results presented here are an application of the procedure in Algorithm 1, which converges on an estimate of the principal axis frame for the giant asteroid.

The spacecraft suffered a safing event during LAMO; the data arc used here (April 9, 2012 - May 10, 2012) was carefully selected to avoid spacecraft safe mode. The solutions use reconstructed spacecraft data based on the actual telemetered events, not prior event predictions.

Figures 7 through 13 show the evolution of the pole and the second-degree harmonics through the iterative convergence procedure. The leftmost black point is the original solution (which processes

but does not estimate the landmark coordinates), and the rightmost gray dot shows the Opnav-estimated solution of the pole parameters. Each parameter has error bars, representing formal 1-sigma confidence levels.

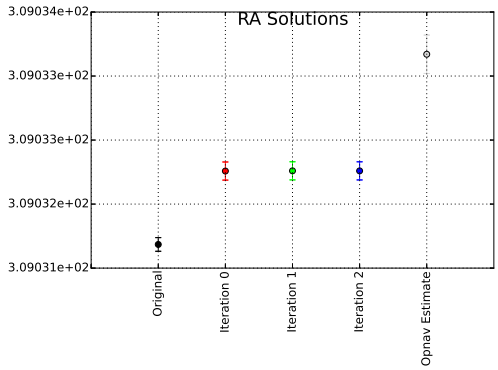

Figure 7: Evolution of the estimation of $\alpha_{p'}$ for Vesta.

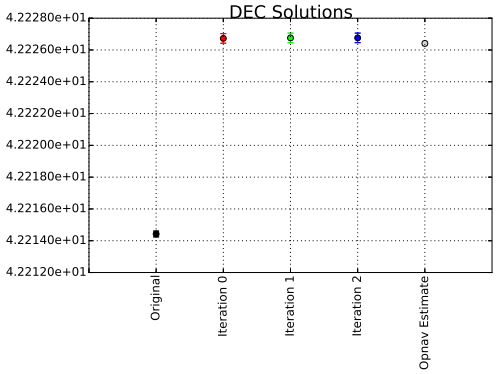

Figure 8: Evolution of the estimation of $\delta_{p'}$ for Vesta.

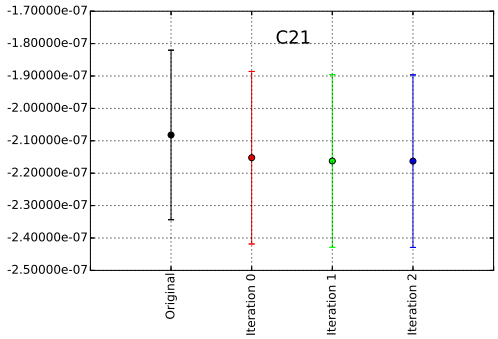

Figure 9: Evolution of the estimation of C_{21} for Vesta.

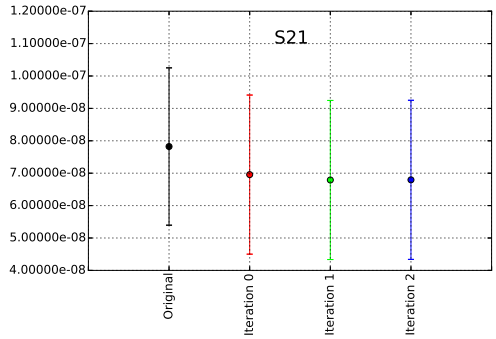

Figure 10: Evolution of the estimation of S_{21} for Vesta.

Through the iterations, each parameter tends toward a particular value. The RA and Dec estimates move toward the Opnav pole from the original OD-estimated pole. This result is specifically interesting when processing Vesta data, as the estimate of the pole location varied widely and inconsistencies between Opnav and OD estimates persisted throughout the operation phase at Vesta.

Of all parameters shown, the behavior of S_{22} in Figure 11 is particularly noteworthy. The estimated value of the original solution is quite far from zero, due to the fact that the Opnav frame is not specifically chosen to align closely with the principal axis frame, and the location of the meridian is geometrically arbitrary. S_{22} is proportional to I_{xy} (see Equation 4), and therefore is a direct estimate of the offset of the body x-axis from the principal x-axis in the xy-plane. At iteration 0, the filter overcorrects S_{22}. However, from iteration 1 and onward, S_{22} converges near zero, indicating that the meridian is successively better aligned with the principal axis frame. The same behavior

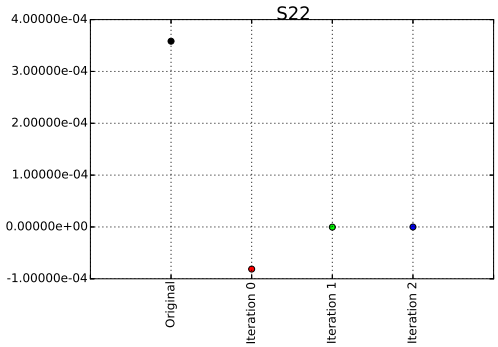

Figure 11: Evolution of the estimation of S_{22} for Vesta.

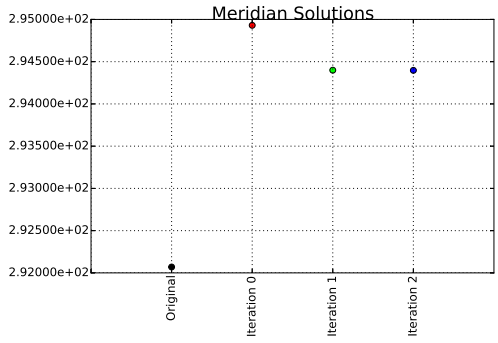

Figure 12: Evolution of the estimation of $W_{p'}$ for Vesta.

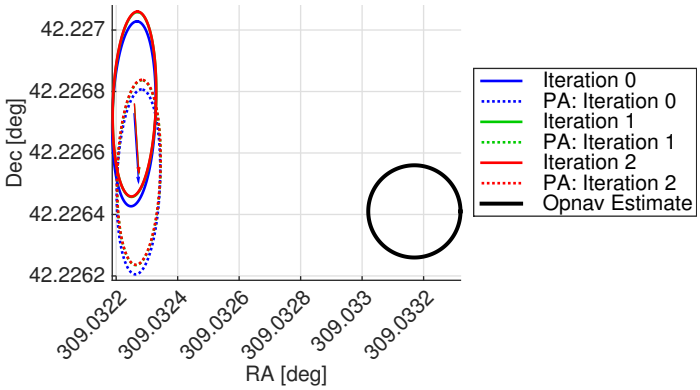

Figure 13: Evolution of the pole estimate for Vesta.

is observed for the evolution of the meridian solutions. It is worthwhile to mention that the total shift of the meridian is merely $\approx 2.5^\circ$. This close alignment of the OD frame with the principal axis frame is sheer coincidence; the Opnav team happened to choose their frame very close to the principal axis frame.

Figure 13 depicts the evolution of the filter solution and the corresponding estimation of the principal axis frame. The solid lines are the filter solutions at each iteration, and each of them has the corresponding principal axis frame estimation that is delineated in a dashed line of the same color (the uncertainty is the same as the filter solution). Iteration 1 immediately determines the pole estimate to within the prescribed 0.01° tolerance. Iteration 2, which is on top of iteration 1 in the figure, proceeds due to the tolerance for the meridian not quite being satisfied. Additionally, the filter solution and the principal axis frame bounce back and forth. The principal axis of the iteration 1 is used as *a priori* for the iteration 2, which re-estimates the same pole. This behavior is manifested in the evolution of the estimates of C_{21}, S_{21}, and S_{22}. Although the estimate of these harmonics does approach zero when the principal axis is found, they do not settle precisely at zero except in a theoretical sense because the data strength in the pole determination has effectively plateaued. This behavior is clearly seen in Figure 13, where the pole estimates from the filter and

from the principal axis correction are within one-sigma of each other. We analyze this behavior more carefully in Section 6.3.

6.2 Ceres Results

Following operations at Vesta and a 32-month interplanetary cruise phase, Dawn arrived at and was captured by Ceres' gravity in March 2015. The mission has progressed in similar order to Vesta operations: approach phase, rotational characterizations, Survey orbit, High Altitude Mapping Orbit (HAMO), and Low Altitude Mapping Orbit (LAMO).[15]

For Ceres operations, we investigate a set of data from the Survey orbit and apply the procedure in Algorithm 1 to converge on an estimate of the principal axis frame for the first dwarf planet ever visited by a spacecraft. Figures 14-20 show nine iterations of the algorithm, operating off of an "original" converged OD case depicted in black. Figures 14, 15, and 20 offer a comparison with the Opnav-derived values for the pole location, depicted in gray.

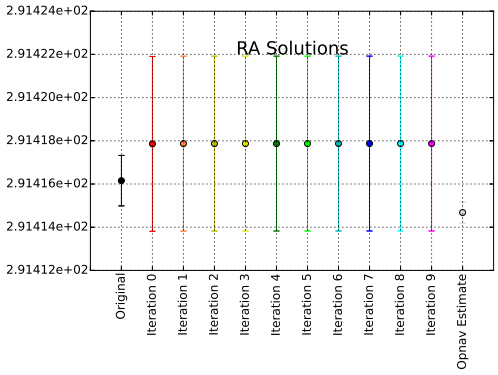

Figure 14: Evolution of the estimation of $\alpha_{p'}$ for Ceres.

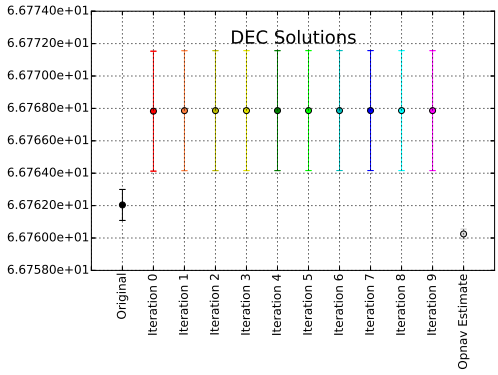

Figure 15: Evolution of the estimation of $\delta_{p'}$ for Ceres.

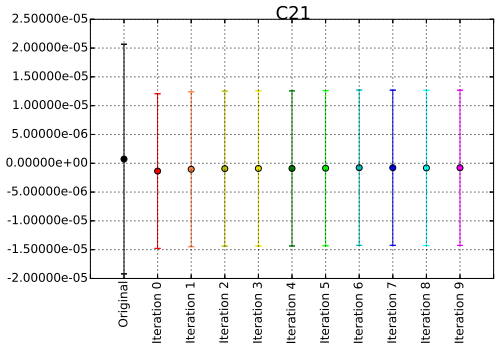

Figure 16: Evolution of the estimation of C_{21} for Ceres.

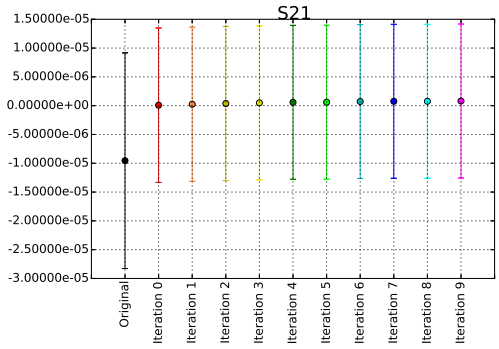

Figure 17: Evolution of the estimation of S_{21} for Ceres.

It is evident that the pole parameters, the meridian, and the harmonics all exhibit an approach to convergence through the iterative process. As stated previously, $C_{21} = S_{21} = S_{22} = 0$ is satisfied

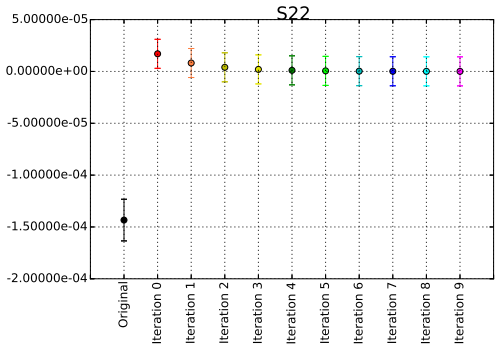

Figure 18: Evolution of the estimation of S_{22} for Ceres.

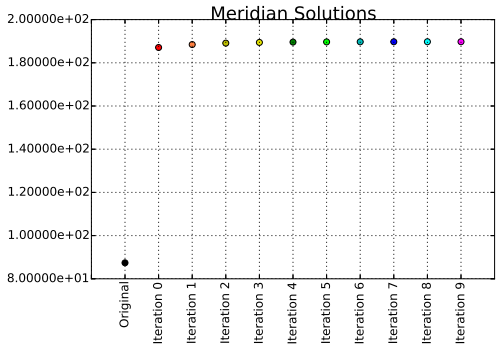

Figure 19: Evolution of the estimation of $W_{p'}$ for Ceres.

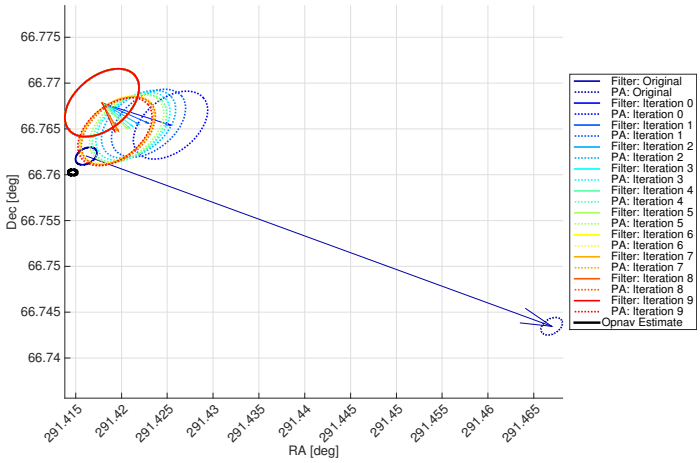

Figure 20: Evolution of the pole estimate for Ceres.

in a theoretical sense as the estimate of the pole and meridian approach the principal axis values. Figures 16, 17, and 18 show the characteristic convergence on a near-zero value as the iterations proceed. Especially noteworthy is the S_{22} progression toward zero in Figure 18. This behavior indicates that the body-fixed x- and y-axes determined with the iterated value of the meridian align well with Ceres' principal axes in the equatorial plane.

Also of note is the trend in the pole solution in Figure 20. With iteration zero (blue), the estimate of the principal axis pole (dashed blue ellipse) jumps immediately away from the original solved-for pole estimate (solid blue ellipse). Through further iterations of the rotation procedure and filtering, the pole location approaches but does not reach the Opnav-supplied estimate, which is approximately 1.5-sigma in variation from the final iteration solution.

Because the data used for this study of Ceres comes from the Survey orbit, the fidelity in gravity term knowledge is not nearly as high as the knowledge is at LAMO. The Vesta LAMO cases, presented in the previous subsection, have a much more confident opinion of the pole location due to their better estimation of C_{21} and S_{21}. The Ceres results for these harmonics parameters, shown in Figures 16 and 17, show that the knowledge does not improve beyond the original generous

one-sigma level of confidence. Nevertheless, the estimate of the harmonics does trend toward zero, indicating a meaningful improvement in knowledge of the pole location.

6.3 Comparison with Statistical Expectation

In both the original and final OD solutions, the knowledge of the solved-for values is subject to statistical uncertainty. We have previously stated the relationship between the second-degree harmonics and the pole location (see Equation 4). The statistical uncertainty in these harmonic parameters is therefore related to the statistical uncertainty in the knowledge of the pole location. To determine how the uncertainty in the harmonics relates to an effective uncertainty in RA and Dec, we employ the same rotation procedure described in Section 3.4 inside of a Monte Carlo scheme. Given the estimated values of the harmonics and their associated uncertainties, samples are repeatedly drawn from the statistical distribution of harmonics values to generate rotation matrices from the OD to the principal axis frame. Each time a rotation is performed, a value of the RA, Dec, and meridian is computed. We repeat the Monte Carlo scheme 10,000 times to obtain a statistical distribution of the uncertainty in the frame given the uncertainty in the spherical harmonics.

Figure 21 shows the result of the Monte Carlo procedure for the Vesta LAMO data arc. The black circle on the right is the Opnav estimate of the pole orientation and its uncertainty. The pole uncertainty due to spherical harmonics uncertainty, computed with the Monte Carlo scheme, is shown as the gray ellipse, which is centered at the pole in the principal axis frame (PA pole) found from the filter solution. The statistical uncertainty computed using the Monte Carlo procedure is nearly identical to the nominal principal axis pole one-sigma error ellipses computed from the filter solution. It is apparent that the nominal values of the filter pole solution and corresponding principal axis pole are within the 1-sigma Monte Carlo error ellipse, showing their statistical equivalency. The Monte Carlo error ellipses do not have an axial tilt because the original sample distribution assumes no correlation between the harmonics values, which results in inflated error ellipse size that is conservative.

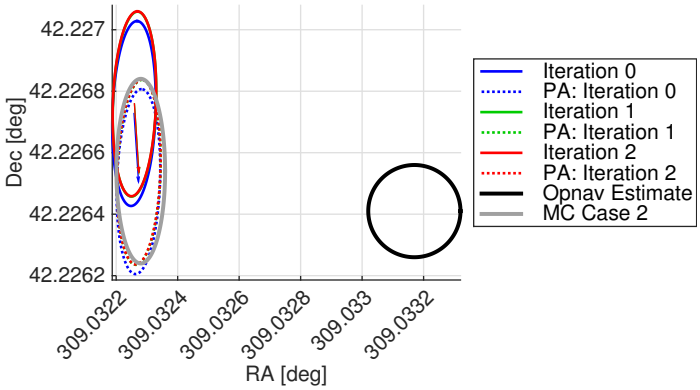

Figure 21: Monte Carlo uncertainty ellipses for Vesta's pole.

Figure 22 shows the result of the Monte Carlo procedure for the Ceres Survey data processing. For the original OD solution, the Monte Carlo pole uncertainty is shown as the dark gray ellipse centered at the principal axis pole estimation of that solution. It is apparent that the uncertainty in the pole due to the uncertainty in the second-degree spherical harmonics is quite large for the data gathered at Survey.

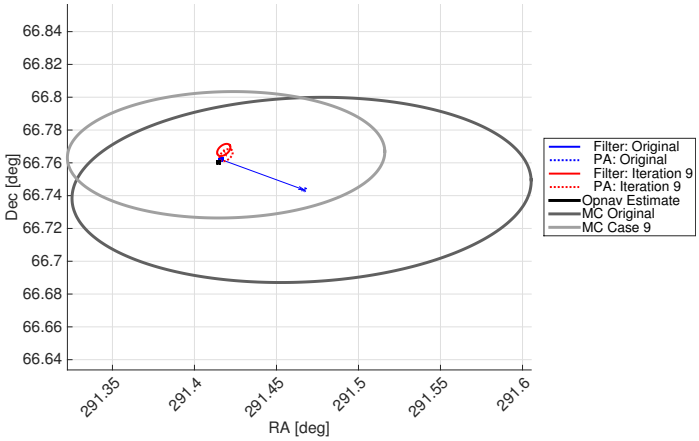

Figure 22: Monte Carlo uncertainty ellipses for Ceres' pole.

The same Monte Carlo procedure is repeated for the final solution (Iteration 9), and is shown as the light gray ellipse in Figure 22. This ellipse is centered around the PA pole for that solution. While the uncertainty is still large compared to the spread of solutions, it has decreased in size compared to the uncertainty of the original OD solution due to the change in the estimated values of the spherical harmonics used to construct the rotation matrix. As the estimate of the off-diagonal terms approach zero, the rotation matrix has less effect on the pole estimate. The relatively small shift in estimates shown in Figure 20 is well within the statistical uncertainty shown in the light gray ellipse.

6.4 Sensitivity of the Pole Parameters to the Nominal Gravity Field

Finally, we investigate the sensitivity of the pole parameters to the nominal values of the second-degree spherical harmonic coefficients. The purpose of this study is to quantify the sensitivity of the RA, Dec, and meridian estimates to the changes in the second-degree harmonic coefficients. Due to each unnormalized spherical harmonic coefficient having different orders of magnitude, we scale the perturbation based on the unnormalized RMS gravity spectrum of the same degree similar to "Kaula's rule":[2]

$$K_n = \sqrt{\frac{\sum_{m=0}^{n} C_{nm}^2 + S_{nm}^2}{2n+1}} \tag{38}$$

The coefficient K_n and the rotation matrix given by the A matrix are heavily dependent on the specifics of each solution run. As an example, we use the final converged solution for the Vesta results shown in Section 6.1 with $K_n = 3.1806 \times 10^{-2}$ for the second degree harmonics. Figures 23-27 show the sensitivity of the PA pole in RA (red), Dec (blue), and meridian (green) with respect to the change in each second-degree harmonic coefficient. In the figures, gravity terms are perturbed according to:

$$\begin{bmatrix} C \\ S \end{bmatrix}_{perturbed} = \begin{bmatrix} C \\ S \end{bmatrix}_{nominal} \pm [\%\ \text{change}] \cdot K_n \tag{39}$$

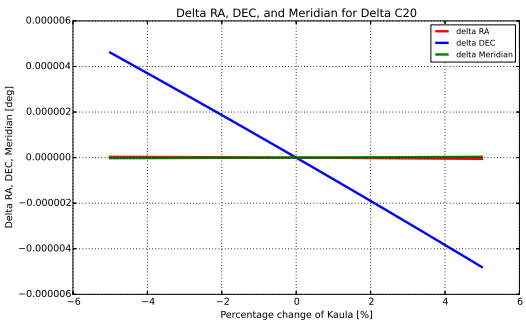

Figure 23: Sensitivity of C_{20} for Vesta April solution.

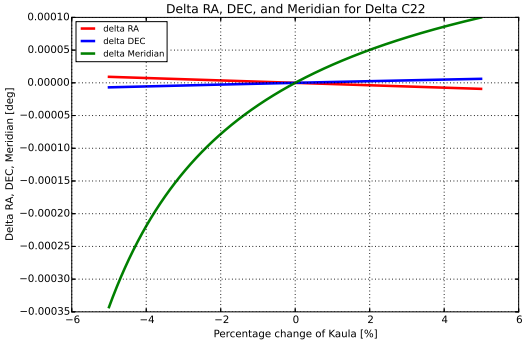

Figure 24: Sensitivity of C_{22} for Vesta April solution.

As shown in Equation 4, the RA and Dec are largely dictated by C_{21} and S_{21}, and meridian is affected by S_{22} with smaller contribution from C_{21} and S_{21}. The Dec and meridian are also affected by C_{20} and C_{22} respectively, but their contributions are significantly smaller than those of the off-diagonal terms. We observe that less than 5% perturbation in gravity spectrum yields $\approx 1^\circ$ shift in RA and Dec for Vesta. Such plots depicting the sensitivity of the pole and meridian to the gravity parameters are useful not only for navigation purposes but also for mission planning purposes, as requirements may be placed on orbital characteristics if the gravity harmonics must be known to within a particular uncertainty to sufficiently estimate the principal axis frame of the target body.

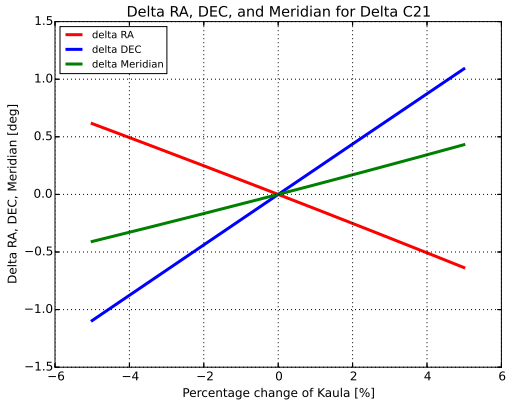

Figure 25: Sensitivity of C_{21} for Vesta April solution.

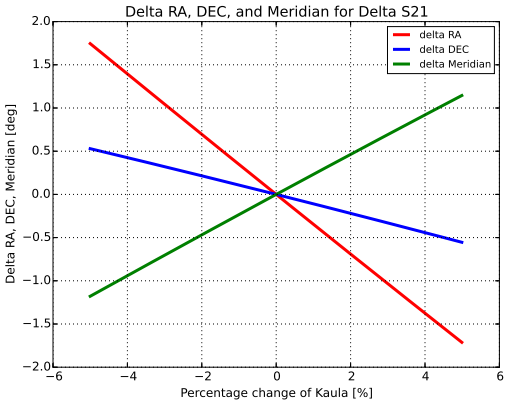

Figure 26: Sensitivity of S_{21} for Vesta April solution.

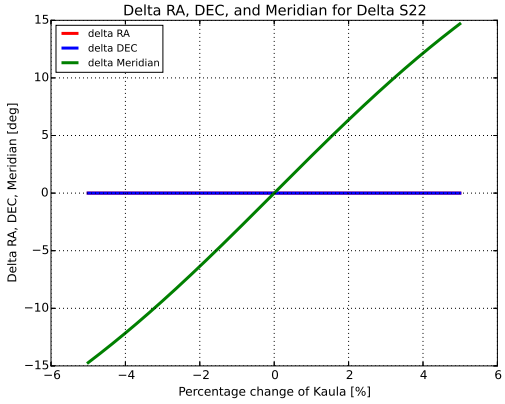

Figure 27: Sensitivity of S_{22} for Vesta April solution.

7 CONCLUSION

The determination of the principal axis frame of a celestial body is important for understanding the body's spin characteristics and density distribution, and for satisfying particular spacecraft orbit geometry requirements. The procedure presented in this manuscript takes advantage of the simultaneous estimation of a body-fixed frame and spherical harmonics coefficients. Through successive iteration and filtering, an improved estimate of the principal axes may be achieved. The procedure is general in nature, and may be applied to any celestial body for which a body-fixed frame is defined and spherical harmonics through degree and order two are sufficiently well-known. The results presented for giant asteroid Vesta and dwarf planet Ceres, both visited by the Dawn mission, show a significant statistical improvement in principal axis frame knowledge using data gathered during mission operations. By tracking the progression of the second-degree spherical harmonics through successive iterations, we verify that the estimation of the principal axis frame does indeed improve.

ACKNOWLEDGMENT

This research was carried out at the Jet Propulsion Laboratory, California Institute of Technology, under a contract with the National Aeronautics and Space Administration.

REFERENCES

[1] Y. Takahashi, M. W. Busch, and D. J. Scheeres, "Spin State and Moment of Inertia Characterization of 4179 Toutatis," *The Astronomical Journal*, Vol. 146, No. 4, 2013.

[2] W. M. Kaula, *Theory of Satellite Geodesy*. Waltham, Massachusetts: Blaisdell Publishing Company, 1966.

[3] E. P. Wigner, *Group Theory and its Application to the Quantum Mechanics of Atomic Spectra*, ch. 15. Academic Press, Inc., 1959.

[4] C. Giacovazzo, *Direct Phasing in Crystallography - Fundamentals and Applications*, ch. 17. Oxford University Press, 1998.

[5] Z. Gimbutas and L. Greengard, "A Fast and Stable Method for Rotating Spherical Harmonic Expansions," *Journal of Computational Physics*, No. 228, 2009, pp. 5621–5627.

[6] M. A. Blanco, M. Flórez, and M. Bermejo, "Evaluation of the Rotation Matrices in the Basis of Real Spherical Harmonics," *Journal of Molecular Structure (Theochem)*, No. 419, 1997, pp. 19–27.

[7] J. Ivanic and K. Ruedenberg, "Rotation Matrices for Real Spherical Harmonics. Direct Determination by Recursion," *Journal of Physical Chemistry*, Vol. 102, 1996, pp. 6342–6347.

[8] J. Ivanic and K. Ruedenberg, "Additions and Corrections: Rotation Matrices for Real Spherical Harmonics. Direct Determination by Recursion," *Journal of Physical Chemistry*, Vol. 102, No. 45, 1998, pp. 9099–9100.

[9] R. Green, "Spherical Harmonic Lighting: The Gritty Details," *Game Developers Conference*, 2003.

[10] M. A. Wieczorek, M. Meschede, and I. Oshchepkov, "SHTOOLS - Tools for Working with Spherical Harmonics," http://shtools.ipgp.fr/, ZENODO, 2015.

[11] B. Kennedy, M. Abrahamson, A. Ardito, R. Haw, N. Mastrodemos, S. Nandi, R. Park, B. Rush, and A. Vaughan, "Dawn Orbit Determination Team: Modeling and Fitting of Optical Data at Vesta," *23rd AAS/AIAA Space Flight Mechanics Meeting*, No. 13-347, 2013.

[12] M. Abrahamson, A. Ardito, D. Han, R. Haw, B. Kennedy, N. Mastrodemos, S. Nandi, R. Park, B. Rush, and A. Vaughan, "Dawn Orbit Determination Team: Trajectory Modeling and Reconstruction Processes at Vesta," *23rd AAS/AIAA Space Flight Mechanics Meeting*, No. 13-479F, 2013.

[13] D. W. Parcher, M. Abrahamson, A. Ardito, D. Han, R. Haw, B. Kennedy, N. Mastrodemos, S. Nandi, R. Park, B. Rush, B. Smith, J. Smith, A. Vaughan, and G. Whiffen, "Dawn Maneuver Design Performance at Vesta," *23rd AAS/AIAA Space Flight Mechanics Meeting*, No. 13-344, 2013.

[14] D. Han, "Orbit Transfers for Dawn's Vesta Operations: Navigation and Mission Design Experience," *23rd International Symposium on Space Flight Dynamics*, 2011.

[15] D. Han, J. Smith, B. Kennedy, N. Mastrodemos, and G. Whiffen, "Orbit Transfers for Dawn's Ceres Operations: Navigation and Mission Design Experience at a Dwarf Planet," *Proceedings of the SpaceOps 2016 Conference*, Daejon, Korea, 2016.